

The HBI in a quasi-global model of the intracluster medium

Henrik N. Latter^{1*}, Matthew W. Kunz^{2,3†}

¹ *Department of Applied Mathematics and Theoretical Physics, University of Cambridge, CMS, Wilberforce Road, Cambridge, CB3 0WA, U. K.*

² *Department of Astrophysical Sciences, 4 Ivy Lane, Peyton Hall, Princeton University, Princeton, NJ 08544, U. S. A.*

³ *Previous Address: Rudolf Peierls Centre for Theoretical Physics, University of Oxford, 1 Keble Road, Oxford, OX1 3NP, U. K.*

ABSTRACT

In this paper we investigate how convective instabilities influence heat conduction in the intracluster medium (ICM) of cool-core galaxy clusters. The ICM is a high-beta, weakly collisional plasma in which the transport of momentum and heat is aligned with the magnetic field. The anisotropy of heat conduction, in particular, gives rise to instabilities that can access energy stored in a temperature gradient of either sign. We focus on the heat-flux buoyancy-driven instability (HBI), which feeds on the outwardly increasing temperature profile of cluster cool cores. Our aim is to elucidate how the global structure of a cluster impacts on the growth and morphology of the linear HBI modes when in the presence of Braginskii viscosity, and ultimately on the ability of the HBI to thermally insulate cores. We employ an idealised quasi-global model, the plane-parallel atmosphere, which captures the essential physics – e.g. the global radial profile of the cluster – while letting the problem remain analytically tractable. Our main result is that the dominant HBI modes are localised to the innermost ($\lesssim 20\%$) regions of cool cores. It is then probable that, in the nonlinear regime, appreciable field-line insulation will be similarly localised. Thus, while radio-mode feedback appears necessary in the central few tens of kpc, heat conduction may be capable of offsetting radiative losses throughout most of a cool core over a significant fraction of the Hubble time. Finally, our linear solutions provide a convenient numerical test for the nonlinear codes that simulate the saturation of such convective instabilities in the presence of anisotropic transport.

Key words: conduction – instabilities – magnetic fields – MHD – plasmas – galaxies: clusters: intracluster medium.

1 INTRODUCTION

Whereas their copious X-ray emission suggests a central cooling time much less than the Hubble time, galaxy cluster cores do not exhibit cooling flows commensurate with their radiative losses. Absent are the mass deposition rates ($\dot{M} \sim 10^2\text{--}10^3 \text{ M}_\odot \text{ yr}^{-1}$) and copious iron line emission that would accompany such flows. Instead, the central temperatures of cool core clusters are typically only $\sim 1/3$ of the bulk cluster temperatures, while spectroscopically determined mass deposition rates are $\lesssim 0.1\dot{M}$ (for a review, see Peterson & Fabian 2006). Understanding how these conditions are maintained in the face of rapid radiative cooling poses a challenge for theorists, who have consequently invoked a plethora of diverse physics to resolve the problem. These include: active galactic nucleus feedback, conductive heat transport, and convective turbulence, whether it be driven by cosmic rays, mergers, or magnetohydrodynamic (MHD) instabilities.

This paper concerns the contribution of conductive heat transport to the solution of the cooling flow problem. However, we do not take the usual energetics standpoint (i.e. does conduction

provide an ample source of heat to offset radiative losses?) but rather focus on how conduction generates, and is subsequently modified by, plasma instabilities and the MHD turbulence they instigate. Because the intracluster medium (ICM) is magnetized and weakly collisional it exhibits surprising stability properties (Balbus 2000, 2001; Schekochihin et al. 2005, 2010). In particular, the outwardly increasing temperature profile of a cluster core gives rise to a heat-flux buoyancy-driven instability (HBI; Quataert 2008) that can drive disordered flows. Numerical simulations show that these flows lead to near-complete field-line insulation of the core, and heat conduction is greatly impeded (Parrish & Quataert 2008; Bogdanović et al. 2009; Parrish, Quataert & Sharma 2009). HBI motions not only seem incapable of maintaining the observed temperature profile (as suggested by Balbus & Reynolds 2008), but actually exacerbate the cooling flow problem. As a result, theorists have appealed to turbulent stirring by other means to reopen the field lines and reinstate the conductive heat-flux (Parrish, Quataert & Sharma 2010; Ruszkowski & Oh 2010; McCourt et al. 2010).

This would bring the issue to a close if it were not for the fact that a magnetized, weakly collisional plasma can exhibit appreciable pressure anisotropy – an effect neglected in most previous work. In fact, HBI modes inevitably generate such anisotropies,

* E-mail: hl278@cam.ac.uk

† E-mail: kunz@astro.princeton.edu; Einstein Postdoctoral Fellow

manifested as viscous stresses, and these adversely affect the instability mechanism. In particular, the wavelengths of the fastest growing modes λ_{HBI} increase from very small scales to those of order the thermal-pressure scaleheight of the cluster H (Kunz 2011). So, even though the HBI mechanism can be understood with local physics, the instability manifests primarily on *global* scales and may be sensitive to the large-scale structure of the cluster, especially via the kinematic viscosity's strong dependence on temperature and density. For this reason, Kunz (2011) conjectured, on account of a WKBJ analysis, that the fastest growing HBI modes would favour only the innermost regions of the cluster core, as it is here that viscous damping is minimised. If the nonlinear saturation of the HBI is similarly confined, then the associated field-line insulation of the core may be significantly attenuated.

In this paper, we investigate how pressure anisotropy and the global structure of the ICM influence the HBI by generalising the linear calculation of Kunz (2011). We calculate the HBI modes in a simple quasi-global model of the cluster: a plane-parallel atmosphere. The model captures the radial density and temperature structure of the ICM, but neglects its angular structure. Though idealized, this model permits us to test in a transparent way the new physics at work, and how the character of the HBI changes in a global setting. In addition, it provides a numerical testbed for nonlinear codes that include anisotropic conduction and viscosity. Our main result is that the dominant HBI modes are typically localised to the innermost ($\lesssim 20\%$) regions of cool-core clusters. It is then likely that, in the nonlinear regime, appreciable field-line insulation will similarly localise and become inefficient. These theoretical results have been corroborated by the Braginskii-MHD simulations presented in Kunz et al. (2012), which use domains sufficiently large to capture this physics.

The paper is organized as follows. In Section 2 we present the model and its governing equations. In Section 3 we derive quasi-global equilibrium solutions to these equations, which are then subjected to linear perturbations in Section 4. There, the HBI eigenmodes are calculated numerically, presented, and discussed. We conclude in Section 5 with a speculative discussion of the implications our results have for the long-term thermal and dynamic stability of cool-core galaxy clusters.

2 FORMULATION OF THE PROBLEM

2.1 Plasma dynamics

The macroscopic scales of the ICM (e.g. the thermal-pressure scale height H) are much greater than the particle mean free path λ_{mfp} and thus a (collisional) MHD description of the ICM plasma remains valid. On the other hand, λ_{mfp} is much larger than the ion gyroradius, a physical regime that ensures the predominance of cyclotron motions. As a consequence, the transport properties of the plasma deviate significantly from what we might expect from classical MHD. For instance, the conduction of heat is strongly anisotropic with respect to the local magnetic field direction, a property that fundamentally alters the ICM's convective stability (Balbus 2000). Temperature gradients, rather than entropy gradients, become the discriminating quantities that determine stability, regardless of whether temperature increases (Balbus 2000, 2001) or decreases (Quataert 2008) in the direction of gravity. In addition, the fluid is subject to pressure anisotropies, i.e. the gas pressure perpendicular p_{\perp} and parallel p_{\parallel} to the local magnetic field may not be equal. Pressure anisotropies arise from the conservation of

the first and second adiabatic invariants of each particle. These ensure that any change in magnetic field strength B and/or density ρ must be accompanied by corresponding changes in p_{\perp} and p_{\parallel} (Chew, Goldberger & Low 1956).

The pressure anisotropy impinges noticeably on the buoyancy instabilities that afflict stratified plasmas, such as the magnetothermal instability (MTI) and the HBI. Because the anisotropy impedes the convergence and divergence of magnetic field lines, the MTI mechanism is strengthened, while the HBI is suppressed. In particular, pressure anisotropy shifts the fastest-growing HBI modes to much longer wavelengths than the very short scales it was thought to favour. In fact, Kunz (2011) finds that the fastest growth occurs for a wavelength $\sim 10(\lambda_{\text{mfp}}H)^{1/2}$, which in the weakly collisional ICM is approximately global, $\sim 0.2H-H$. These longer modes operate on a timescale slower than conduction but faster than viscous diffusion; thus they can effectively access free energy via the heat-flux, while minimising viscous damping.

Pressure anisotropies also give rise to a host of ‘microinstabilities’, which include the firehose, mirror, and gyrothermal instabilities (Schekochihin et al. 2005, 2010). These generate turbulent fluctuations on ‘nano-scales’ of ~ 10 npc and ~ 10 hr, which likely set the pressure anisotropy and heat-fluxes on the larger scales that the HBI inhabits (Schekochihin et al. 2010). Ideally, these fluctuations would be ‘smoothed out’ by a mean field theory or else accounted for in some fashion. In this work we assume from the outset that our plasma is Maxwellian, and so these instabilities do not appear in our linear theory (though they may during the nonlinear phase of the evolution).

2.2 Governing equations

The model we use is that of Braginskii-MHD, in which the equations of classical MHD are employed but with special prescriptions (closures) for the transport of momentum and heat (Braginskii 1965). The evolutionary equations governing the mass density ρ , velocity \mathbf{v} , dimensionless entropy $S = \ln(\rho^{-5/3}p)$, and magnetic field \mathbf{B} are, respectively,

$$\frac{D\rho}{Dt} = -\rho\nabla\cdot\mathbf{v}, \quad (1)$$

$$\frac{D\mathbf{v}}{Dt} = \mathbf{g} - \frac{1}{\rho}\nabla\left(\mathbf{P} + \mathbf{I}\frac{B^2}{8\pi} - \frac{\mathbf{B}\mathbf{B}}{4\pi}\right), \quad (2)$$

$$\frac{3}{2}p\frac{DS}{Dt} = \Gamma - \Lambda - \nabla\cdot\mathbf{q}, \quad (3)$$

$$\frac{D\mathbf{B}}{Dt} = \mathbf{B}\cdot\nabla\mathbf{v} - \mathbf{B}\nabla\cdot\mathbf{v}, \quad (4)$$

where

$$\frac{D}{Dt} \equiv \frac{\partial}{\partial t} + \mathbf{v}\cdot\nabla \quad (5)$$

is the convective (Lagrangian) derivative, \mathbf{g} is the gravitational acceleration, and \mathbf{P} is the (thermal) pressure tensor with the isotropic pressure defined through $p = (1/3)\text{Tr}\mathbf{P}$. The viscous heating rate is Γ , the radiative cooling rate is Λ , and \mathbf{q} is the conductive heat-flux. In addition, the magnetic field must satisfy $\nabla\cdot\mathbf{B} = 0$. Throughout we assume that the gas satisfies the ideal gas law $p = \rho v_{\text{th}}^2$, where $v_{\text{th}}^2 = 2k_{\text{B}}T/m_{\text{p}}$ is the thermal speed of the ions (with k_{B} denoting the Boltzmann constant and m_{p} proton mass). The adiabatic index γ has been set to $5/3$. We consider a

hydrogenic plasma with equal ion and electron number densities, $n_i = n_e$, and temperatures, $T_i = T_e = T$.

2.2.1 Pressure tensor

The ICM plasma distribution function is gyrotropic. As a consequence, the pressure tensor reduces to:

$$\mathbf{P} = p_{\perp}(\mathbf{I} - \hat{\mathbf{b}}\hat{\mathbf{b}}) + p_{\parallel}\hat{\mathbf{b}}\hat{\mathbf{b}}, \quad (6)$$

where $\hat{\mathbf{b}} = \mathbf{B}/B$, and p_{\perp} and p_{\parallel} are the pressures perpendicular and parallel to the local magnetic field. The total gas pressure is

$$p = \frac{2}{3}p_{\perp} + \frac{1}{3}p_{\parallel}. \quad (7)$$

When the ion-ion collision time τ_{ii} is much shorter than the characteristic timescales associated with the macroscopic fields, the pressure anisotropy may be computed from

$$p_{\perp} - p_{\parallel} = 0.960 p_i \tau_{ii} \frac{d}{dt} \ln \frac{B^3}{\rho^2}. \quad (8)$$

Here we have ignored the contribution of the electrons, which is a factor $\sim(m_e/m_i)^{1/2}$ smaller than that of the ions (Catto & Simakov 2004). By using equations (1) and (4) to replace the time derivatives of density and magnetic field strength with velocity gradients, equation (8) may be written as

$$p_{\perp} - p_{\parallel} = 3\rho\nu \left(\hat{\mathbf{b}}\hat{\mathbf{b}} - \frac{1}{3}\mathbf{I} \right) : \nabla \mathbf{v}, \quad (9)$$

where we have introduced the (kinematic) viscosity coefficient

$$\begin{aligned} \nu &\equiv 0.960 \times \frac{1}{2} v_{th}^2 \tau_{ii}, \\ &\simeq 0.031 \left(\frac{n_i}{0.01 \text{ cm}^{-3}} \right)^{-1} \left(\frac{k_B T}{2 \text{ keV}} \right)^{5/2} \text{ kpc}^2 \text{ Myr}^{-1}. \end{aligned} \quad (10)$$

This pressure anisotropy is the physical effect behind what is known as Braginskii (1965) viscosity – the restriction of the viscous damping to the motions and gradients parallel to the magnetic field.

Other than impeding motions in the momentum equation (2), the Braginskii stress appears in the entropy equation (3) through the viscous heating term, Γ . Using the closure (8), this heating term is $\propto \nu_{ii}(p_{\perp} - p_{\parallel})^2$ and is therefore higher order in the linear analysis we perform.

2.2.2 Heat conduction

When the particle gyroradius is much smaller than the collisional mean free path, heat is restricted to flow along magnetic lines of force (e.g. Braginskii 1965). The heat-flux can then be written as

$$\mathbf{q} = -\rho\kappa \hat{\mathbf{b}}\hat{\mathbf{b}} \cdot \nabla v_{th}^2. \quad (11)$$

The parallel thermal diffusivity κ is dominated by the contribution from the electrons,

$$\begin{aligned} \kappa &\equiv 1.581 \times \frac{1}{2} v_{th,e}^2 \tau_{ee} \\ &\simeq 1.67 \left(\frac{n_i}{0.01 \text{ cm}^{-3}} \right)^{-1} \left(\frac{k_B T}{2 \text{ keV}} \right)^{5/2} \text{ kpc}^2 \text{ Myr}^{-1}, \end{aligned} \quad (12)$$

where $v_{th,e}^2 = 2k_B T/m_e$ is the thermal speed of the electrons and τ_{ee} is the electron-electron collision time (Catto & Simakov 2004). The parallel thermal diffusivity of the ions is a factor

$\sim(m_e/m_i)^{1/2}$ smaller (Spitzer 1962). For future reference, we also define the (Spitzer) parallel thermal conductivity

$$\chi = (p/T)\kappa. \quad (13)$$

2.2.3 Radiative cooling

The second term on the right side of (3) is the radiative cooling rate function Λ . We adopt thermal Bremsstrahlung radiation, and take Λ to be

$$\Lambda = 10^{-27} \left(\frac{n_i}{0.01 \text{ cm}^{-3}} \right)^2 \left(\frac{k_B T}{2 \text{ keV}} \right)^{1/2} \text{ ergs cm}^{-3} \text{ s}^{-1} \quad (14)$$

(Rybicki & Lightman 1979). The cooling in the ICM is dominated by Bremsstrahlung above temperatures $\sim 1 \text{ keV}$.

2.3 Model geometry

The stability calculation requires us to set up a suitable geometry and background magnetic field configuration. Galaxy clusters are approximately spherical, but in this geometry it is unclear what the most appropriate (or analytically feasible) configuration the magnetic field should take. Previous linear theory has sidestepped these issues by employing a local model, in which the magnetic field may take a simple form (purely vertical, for instance). However, in this paper we explicitly wish to test the importance of global structure when in the presence of Braginskii viscosity (Kunz 2011). We hence employ an intermediate model, the plane-parallel atmosphere (see e.g. Lamb 1997), used frequently in stellar convection problems (Hurlburt et al. 1989; Brandenburg et al. 1996). This is an idealised physical system, but one that can help isolate features associated with a cluster's global radial structure while evading the uncertainties and analytic difficulties of magnetic field configurations in spherical geometry. Though our model poorly describes a cluster in its full complexity, it should nevertheless exhibit its salient physics, shared by more advanced models.

The plane-parallel atmosphere is an approximation to a chunk of the spherical cluster. Terms arising from spherical geometry are dropped; angular structure is neglected but the radial structure is retained. Put another way, the model is local in the angular (i.e. horizontal, x, y) directions and global in the radial (i.e. vertical, z). We adopt a uniform gravitational acceleration in the vertical direction, $\mathbf{g} = -g\hat{\mathbf{z}}$. The vertical extent of the layer is taken to be finite and conditions need to be applied at its upper and lower boundaries, which occur at $z = 0$ and $z = Z$. Finally, the background magnetic field is assumed to be constant and vertical within the layer. The plane-parallel atmosphere is well-suited to the morphology of the HBI modes in this set-up because these possess small radial and large horizontal wavenumbers (Kunz 2011). The 'quasi-global' plane-parallel atmosphere works best in the outskirts of the cool core: neglecting the geometric spherical terms introduce errors of order Z/r . However, these errors we believe will not alter the qualitative behaviour revealed by our calculations.

3 EQUILIBRIUM STATE

We consider a static Maxwellian plasma vertically-stratified in both density $\rho(z)$ and temperature $T(z)$, threaded by a uniform background magnetic field oriented along $\hat{\mathbf{z}}$. We further assume that the ratio of the thermal and magnetic pressure is large:

$$\beta \equiv \frac{8\pi p}{B^2} = \frac{2v_{th}^2}{v_A^2} \gg 1, \quad (15)$$

where $v_A \equiv B/(4\pi\rho)^{1/2}$ is the Alfvén speed. Faraday rotation measurements suggest $\beta \sim 10^2\text{--}10^4$ in the cool cores of galaxy clusters (for a review, see Carilli & Taylor 2002).

The equilibrium must satisfy force and energy balances

$$\frac{dp}{dz} = -g\rho \quad \text{and} \quad \frac{dq}{dz} = -\Lambda, \quad (16)$$

where the heat-flux in the background state is given by

$$q = -\chi \frac{dT}{dz}. \quad (17)$$

We consider two thermal equilibria: one in which there is no cooling, $\Lambda = 0$, and hence no conductive heating; and one in which $\Lambda \neq 0$ and Bremsstrahlung radiation balances conductive heating.

Finally, thermal boundary conditions need to be applied at the upper and lower boundaries of the layer, at $z = 0$ and $z = Z$. Various boundary conditions may be invoked, but we choose the simplest: we force the top and bottom layers to have fixed temperatures: $T(0) = T_0$ and $T(Z) = T_Z$.

3.1 No cooling: $\Lambda = 0$

In order to preserve thermal equilibrium when cooling is absent, the background heat-flux must be constant:

$$\frac{d}{dz} \left(\chi \frac{dT}{dz} \right) = 0. \quad (18)$$

Enforcing the boundary conditions, equation (18) may be integrated to yield the temperature profile

$$T(z) = T_0 \left(1 + \zeta \frac{z}{Z} \right)^{2/7}, \quad (19)$$

where $\zeta = [(T_Z/T_0)^{7/2} - 1]$ measures the magnitude of the constant heat-flux through the atmosphere ($q \propto -\zeta$). Combining this result with equation (16) determines the pressure profile

$$p(z) = p_0 \exp \left\{ -\frac{7}{5} \frac{Z}{\zeta H_0} \left[\left(1 + \zeta \frac{z}{Z} \right)^{5/7} - 1 \right] \right\}, \quad (20)$$

where

$$H_0 = v_{\text{th},0}^2/g \quad (21)$$

is the thermal-pressure scale height at $z = 0$, and p_0 is the pressure at $z = 0$. The density follows from the equation of state.

This equilibrium is characterized by two dimensionless parameters: ζ , which is $\sim 10\text{--}50$ in typical cool-core clusters, and

$$\mathcal{G} \equiv \frac{Z}{H_0} \quad (22)$$

which is a measure of the vertical extent of the layer. One example of this atmosphere with $T_Z/T_0 = 2.5$ (i.e. $\zeta \simeq 23.7$) and $\mathcal{G} = 2$ is shown in Figure 1 as the red lines.

3.2 Bremsstrahlung cooling: $\Lambda \propto \rho^2 T^{1/2}$

When Bremsstrahlung cooling is present, no analytic solution exists. Instead, we employ a shooting method to solve equations (16)–(17), subject to three boundary conditions: $T = T_0$ and $\rho = \rho_0$ at $z = 0$, and $T = T_Z$ at $z = Z$. The presence of cooling introduces another dimensionless free parameter,

$$S \equiv \frac{(\Lambda/p)_0}{\kappa_0/Z^2} \simeq 18.4 \left(\frac{Z}{250 \text{ kpc}} \right)^2 \left(\frac{n_{i,0}}{0.01 \text{ cm}^{-3}} \right)^2 \left(\frac{k_B T_0}{2 \text{ keV}} \right)^{-3}, \quad (23)$$

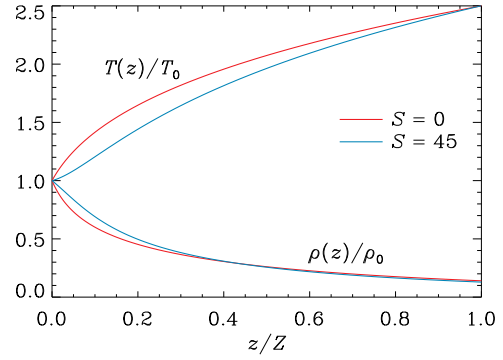


Figure 1. Equilibrium atmospheres with (blue lines) and without (red lines) Bremsstrahlung cooling for $T_Z/T_0 = 2.5$ (i.e. $\zeta \simeq 23.7$) and $\mathcal{G} = 2$.

which is the ratio of the radiative diffusion time (across a distance Z) and the characteristic cooling time (each evaluated at $z = 0$). S is related to the Stefan number (Sf) used in some convection studies. If we scale space by Z , ρ by ρ_0 , and T by T_0 , the equations can be written in the following form, suitable for numerical work:

$$\frac{dq}{dz} = -S\rho^2 T^{1/2}, \quad (24)$$

$$\frac{dT}{dz} = -qT^{-5/2}, \quad (25)$$

$$\frac{d\rho}{dz} = -\mathcal{G}\rho T^{-1} + \rho q T^{-7/2}. \quad (26)$$

The boundary conditions are hence $\rho(0) = 1$, $T(0) = 1$ and $T(Z) = (T_Z/T_0)$. Note that in the limit of small S (ineffective radiative cooling), the first equation gives a constant q to leading order and we recover the ‘no-cooling’ solution of the previous subsection.

Figure 1 describes an example of a cooling atmosphere with $T_Z/T_0 = 2.5$ (i.e. $\zeta \simeq 23.7$), $\mathcal{G} = 2$, and $S = 45$, plotted with the blue lines. This atmosphere is very similar to the cool core of A85, particularly for $z \gtrsim 50$ kpc (Cavagnolo et al. 2009). Note that the effects of cooling are localised to relatively small z , where the density is greatest. As a result, the heat conduction q (not plotted) is attenuated at these z , dropping to approximately zero at $z = 0$. The gradient of the temperature follows, via (17), and is hence flatter than in the non-cooling atmosphere.

4 LINEAR MODES

4.1 Linearised equations

We consider two-dimensional perturbations, $\delta\rho$, δT , $\delta\mathbf{B}$, and $\delta\mathbf{v}$, upon our equilibrium state that exhibit a space-time dependence $\propto f(z) \exp(\sigma t + ikx)$, where σ is a (complex) growth rate and k a (real) wavenumber. Such modes are local in the direction perpendicular to the background magnetic field (\hat{x}) and global in the direction along the background magnetic field (\hat{z}). Because the modes are two-dimensional, it is convenient to use the magnetic flux function A defined through $\mathbf{B} = \nabla \times (A \hat{y})$. Finally, we scale space by Z , speed by $v_{\text{th},0}$, density by ρ_0 , temperature by T_0 , and the flux function by $B_0 Z$. Time, as a consequence, is scaled by $Z/v_{\text{th},0}$.

The governing equations, written to linear order in the perturbation amplitudes, are then

$$\sigma \frac{\delta \rho}{\rho} = -ik\delta v_x - \left(\frac{d \ln \rho}{dz} + \frac{\partial}{\partial z} \right) \delta v_z, \quad (27)$$

$$\begin{aligned} \sigma \delta v_x = & -ikT \left(\frac{\delta \rho}{\rho} + \frac{\delta T}{T} \right) + \frac{2}{\beta_0 \rho} \left(k^2 - \frac{\partial^2}{\partial z^2} \right) \delta A \\ & - \frac{ik}{\text{Re}} \frac{T^{5/2}}{\rho} \left(\frac{2}{3} \frac{\partial \delta v_z}{\partial z} - \frac{1}{3} ik\delta v_x \right), \end{aligned} \quad (28)$$

$$\begin{aligned} \sigma \delta v_z = & -T \frac{\partial}{\partial z} \frac{\delta \rho}{\rho} - \left(T \frac{d \ln p}{dz} + T \frac{\partial}{\partial z} \right) \frac{\delta T}{T} \\ & + \frac{2}{\text{Re}} \frac{T^{5/2}}{\rho} \left(\frac{5}{2} \frac{d \ln T}{dz} + \frac{\partial}{\partial z} \right) \left(\frac{2}{3} \frac{\partial \delta v_z}{\partial z} - \frac{1}{3} ik\delta v_x \right), \end{aligned} \quad (29)$$

$$\begin{aligned} \sigma \frac{3}{2} \frac{\delta T}{T} = & -ik\delta v_x - \left(\frac{3}{2} \frac{d \ln T}{dz} + \frac{\partial}{\partial z} \right) \delta v_z \\ & + \frac{1}{p \text{Pe}} \left[\frac{\partial^2}{\partial z^2} \left(T^{7/2} \frac{\delta T}{T} \right) + ikq \frac{\partial \delta A}{\partial z} - \mathcal{S} \delta \Lambda \right], \end{aligned} \quad (30)$$

$$\sigma \delta A = -\delta v_x, \quad (31)$$

where

$$\delta \Lambda = \Lambda \left(2 \frac{\delta \rho}{\rho} + \frac{1}{2} \frac{\delta T}{T} \right). \quad (32)$$

These equations introduce three dimensionless parameters: the plasma beta at $z = 0$, denoted by β_0 , and the Reynolds and Peclet numbers at $z = 0$, defined through

$$\text{Re} = \frac{Z v_{\text{th},0}}{\nu_0} \quad \text{and} \quad \text{Pe} = \frac{Z v_{\text{th},0}}{\kappa_0}, \quad (33)$$

which quantify the relative importance of viscous and thermal transport, respectively. In the context of the ICM, both numbers can be replaced by a single parameter, the inverse Knudsen number at $z = 0$, defined through

$$\begin{aligned} \text{Kn}_0^{-1} & \equiv \frac{H_0}{\lambda_{\text{mfp},0}} \\ & \simeq 1207 \left(\frac{g}{10^{-8} \text{ cm s}^{-2}} \right)^{-1} \left(\frac{n_{i,0}}{0.01 \text{ cm}^{-3}} \right) \left(\frac{k_B T_0}{2 \text{ keV}} \right)^{-1}. \end{aligned} \quad (34)$$

The Knudsen number is simply the ratio of the mean free path to the scale height. We find that

$$\text{Re} = 2.08 \mathcal{G} \text{Kn}_0^{-1} \quad \text{and} \quad \text{Pe} = 0.042 \mathcal{G} \text{Kn}_0^{-1}. \quad (35)$$

There are hence six dimensionless parameters that fully specify the problem. The equilibrium is set by ξ , \mathcal{G} , and \mathcal{S} , while the linear analysis introduces β_0 , Kn_0 , and the (scaled) horizontal wavenumber k .

Finally, the Prandtl number may be written as

$$\text{Pr} \equiv \frac{\nu_0}{\kappa_0} = 0.607 \frac{\Lambda_e}{\Lambda_i} \left(\frac{2m_e}{m_i} \right)^{1/2} \simeq 0.02. \quad (36)$$

Though Pr does not appear explicitly in the governing equations it is still of interest. Note that Pr is roughly constant. This implies that viscous forces operate on a timescale τ_{visc} that is a fixed number larger than the timescale on which conduction operates, τ_{cond} . For the approximately incompressible perturbations examined in this paper, $\tau_{\text{visc}}/\tau_{\text{cond}} = (2/15)\text{Pr}^{-1} \approx 6$ (Kunz 2011).

4.1.1 Boundary conditions

This set of coupled ordinary differential equations must be solved over the domain $z = [0, 1]$ subject to boundary conditions. We first assume that there is no penetration through the upper and lower boundaries of the atmosphere, and so $\delta v_z = 0$ at $z = 0$ and 1 . In addition, the magnetic field is constrained to be purely vertical at the boundaries: $d\delta A/dz = 0$ at $z = 0, 1$. Now, if we enforce constant temperatures T_0 and T_Z at $z = 0, 1$, then we must also have zero temperature fluctuations at the boundary, $\delta T = 0$. This boundary condition is used in most numerical studies of the HBI in plane-parallel geometry and is the simplest to implement. Other conditions were trialed, such as zero heat-flux perturbation on the lower boundary, with little change in the qualitative results.

4.2 Numerical scheme

We solve equations (27)–(29) numerically via a pseudospectral technique. The z -domain is partitioned into a Gauss-Lobatto grid with $N = 250$ grid points and the differential operator is discretized as a (Chebyshev) derivative matrix (Boyd 2000). A $5N \times 5N$ matrix equation ensues taking the form of a generalised algebraic eigenvalue problem; this yields a spectrum that approximates that of the original differential operator. The eigenvalues σ are obtained using standard linear algebra routines such as the QZ algorithm or an Arnoldi method (Golub & van Loan 1996).

4.3 Results

We present results for various parameters. Throughout, however, we set $\mathcal{G} = 2$, $T_Z/T_0 = 2.5$ (or equivalently $\zeta = 23.7$). This leaves the cooling parameter \mathcal{S} , which we either assign to be 0 or 45; the plasma beta at the lower boundary $\beta_0 = 10^5$; and the inverse Knudsen number Kn_0^{-1} , which we take usually to be 1500. Finally, the horizontal wavenumber k ranges between 0 and 1000.

4.3.1 Growth rates

On account of the finite vertical domain of the layer, there are a discrete number of HBI modes each with a distinct vertical structure, as opposed to the k_z continuum exhibited by the local model. The fastest growing of these modes undergo the least vertical variation (corresponding roughly to smaller k_z in the local analysis), while the slowest growing modes exhibit much finer-scale structure (larger k_z).

In Fig. 2 the growth rates of the leading modes are plotted against horizontal wavenumber k for the non-cooling and cooling cases. In accord with the local analysis, we find that the fastest-growing HBI modes have large horizontal (perpendicular) wavenumber, with $kZ \gtrsim 3\mathcal{G}\text{Kn}_0^{-1/2}$ (see figure 3 of Kunz 2011). This wave configuration maximizes convergence/divergence of the background heat-flux and the consequent heating/cooling of the plasma. Modes on arbitrarily small horizontal scales grow at the maximum rate, and so the system is ill-posed unless these small scales are regularised via the inclusion of finite Larmor radius (FLR) effects, for example. Conversely, most modes are extinguished for sufficiently small k (long horizontal wavelengths): an HBI mode ceases to grow efficiently when its horizontal wavelength becomes much longer than its characteristic vertical scale. The concentration of the heat-flux becomes inefficient in this case.

The magnitude of the growth rates that appear in Fig. 2 is typical for sensible parameter choices. The peak e-folding times are

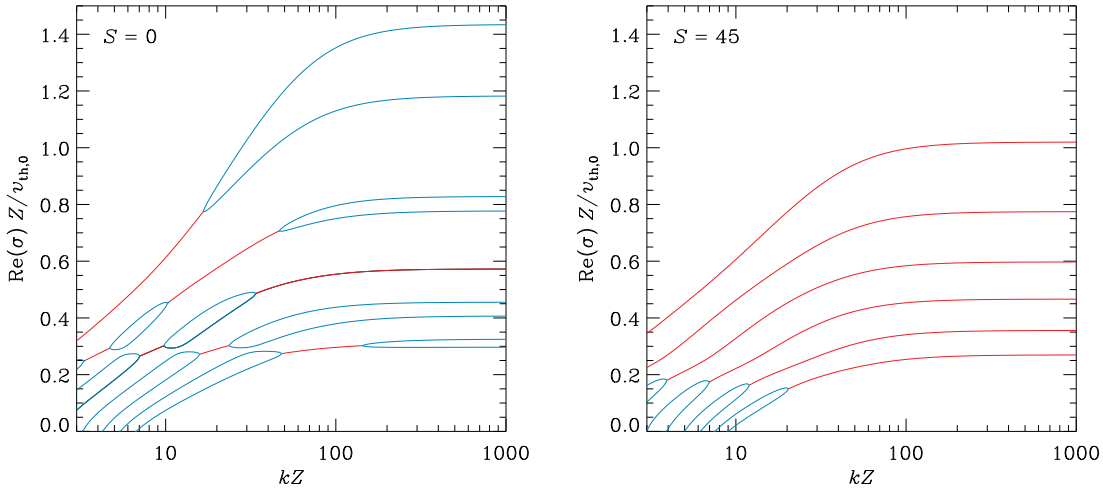


Figure 2. Growth rates of various HBI modes as functions of the perpendicular wavenumber k . The parameters of the system are: $T_Z/T_0 = 2.5$, $G = 2$, $\beta_0 = 10^5$, and $\text{Kn}_0^{-1} = 1500$. The left panel corresponds to the non-cooling case $S = 0$, the right panel to $S = 45$. The growth rates are either purely real (blue lines) or come in complex conjugate pairs (red lines). Note that there exist multiple bifurcations at which conjugate pairs ‘detach’ and become purely monotonic modes, or two monotonic modes coalesce and form a conjugate pair. The cooling case appears to favour oscillatory growth (complex conjugate pairs), especially for large k .

roughly $Z/v_{th,0} \approx 400$ Myr for $Z = 250$ kpc and $k_B T_0 = 2$ keV. As β_0 is lowered, slower-growing modes, which exhibit finer vertical structure, are stabilised because the Alfvén length reaches their characteristic lengthscales and magnetic tension comes into play. For instance, when $kZ = 300$ and $\beta_0 = 10^5$ (with no cooling) there are 32 growing modes; but when β_0 is decreased to 10^4 this number drops to 14, and then to 5 when $\beta_0 = 10^3$. Greater magnetic tension (lower β_0) also lowers the maximum growth rate.

Unstable HBI modes can exhibit either monotonic or oscillatory growth analogous to magnetoconvection in a finite layer (e.g. Proctor & Weiss 1982). In the case of oscillatory growth, modes occur in complex conjugate pairs. As k (or Kn_0) varies, bifurcations occur where conjugate pairs ‘detach’ and become purely monotonic modes, or monotonic modes coalesce and transform into conjugate pairs. In Fig. 2 these two modes are represented by either blue (purely real) or red (complex) lines. This behaviour should be contrasted to the local analysis in which the HBI is always monotonically growing. It follows, in part, from the variation in the background temperature and, in particular, its influence on the thermal conductivity. In a global model the perturbed heat flux introduces a term proportional to $(dT/dz)\delta\chi \propto (dT/dz)\delta T$, which is absent from a local analysis. Under the right conditions, this term can facilitate growth by injecting the free energy from the gradient into a thermodynamic wave during its ‘compressed’ phase. Interestingly, in a radiatively cooling atmosphere growing modes tend to favour the oscillatory form. Cooling accentuates local perturbations in δT and thus reinforces the oscillatory response of the perturbed heat flux.

4.3.2 Eigenfunctions

In Fig. 3 we show the four fastest-growing eigenmodes for $S = 0$, $\text{Kn}_0^{-1} = 1500$, and $\beta_0 = 10^5$. The horizontal wavenumber $k = 250$. We plot their Lagrangian displacements, ξ_x and ξ_z , the scaled density $\delta\rho/\rho$ and temperature $\delta T/T$, as well as the perturbed magnetic-field lines.

What is most striking in these plots is that the the fastest-growing modes, which should dominate the driving of nonlinear

disordered flows, are confined to the innermost $\sim 20\%$ of the atmosphere, as presaged by the local WKB approach (Kunz 2011). There are two reasons for this. First, because the HBI growth rate is proportional to $(d \ln T / d \ln z)^{1/2}$, these modes take advantage of the steeper temperature gradient at small z . Indeed, the local growth rate is a factor $\zeta^{1/2} \approx 5$ less at the top of the layer than it is at the bottom. Second, because the kinematic viscosity is $\nu \propto T^{5/2}/\rho$, the higher temperatures and lower densities characteristic of the upper portion of the atmosphere guarantee rapid viscous damping of wavelengths significantly smaller than the local thermal-pressure scale height. This is also the cause of the relatively straight field lines for $z \gtrsim 0.2Z$ for all of the shown eigenmodes. As a consequence of these two effects, the degree of confinement depends on the parameters (T_Z/T_0) and Kn_0 . We find that the fraction of the atmosphere perturbed by the fastest growing mode scales like $(T_Z/T_0)^{-5/2} \text{Kn}_0^{1/2}$ for $\text{Kn}_0 > 1/3000$. The dependence on Kn_0 here coincides, unsurprisingly, with the HBI’s favoured vertical wavelength in the local analysis (Kunz 2011).

Slower growing modes (not shown) exhibit greater variation (i.e. more nodes) and extend farther into the atmosphere. Yet only the very slowest modes exhibit significant perturbations throughout the entire layer. For example, a typical e-folding time for the growth of substantial magnetic structures at large z is $\gtrsim 5$ Gyr, an order of magnitude longer than the peak e-folding time. Consequently, it is unlikely that such modes are dynamically important during the nonlinear saturation of the HBI.

Figure 4 presents the four fastest-growing eigenmodes for the same parameters as in Fig. 3, except that $S = 45$. These modes occur in complex conjugate pairs, but we plot only one member of the pair. The modes’ morphologies are qualitatively the same as in the non-cooling case; however the localisation is less pronounced. This is due in part because the equilibrium temperature gradient and heat-flux are smaller at low z when cooling is present. Thus both the free energy source and the catalyst for instability are diminished. To compensate, the mode ‘spreads out’ to access as much energy as viscous damping permits. Nonetheless, maximum HBI growth rates suffer and drop, in relative terms, by roughly a third (cf. Fig. 2). As with the non-cooling atmosphere, the growth

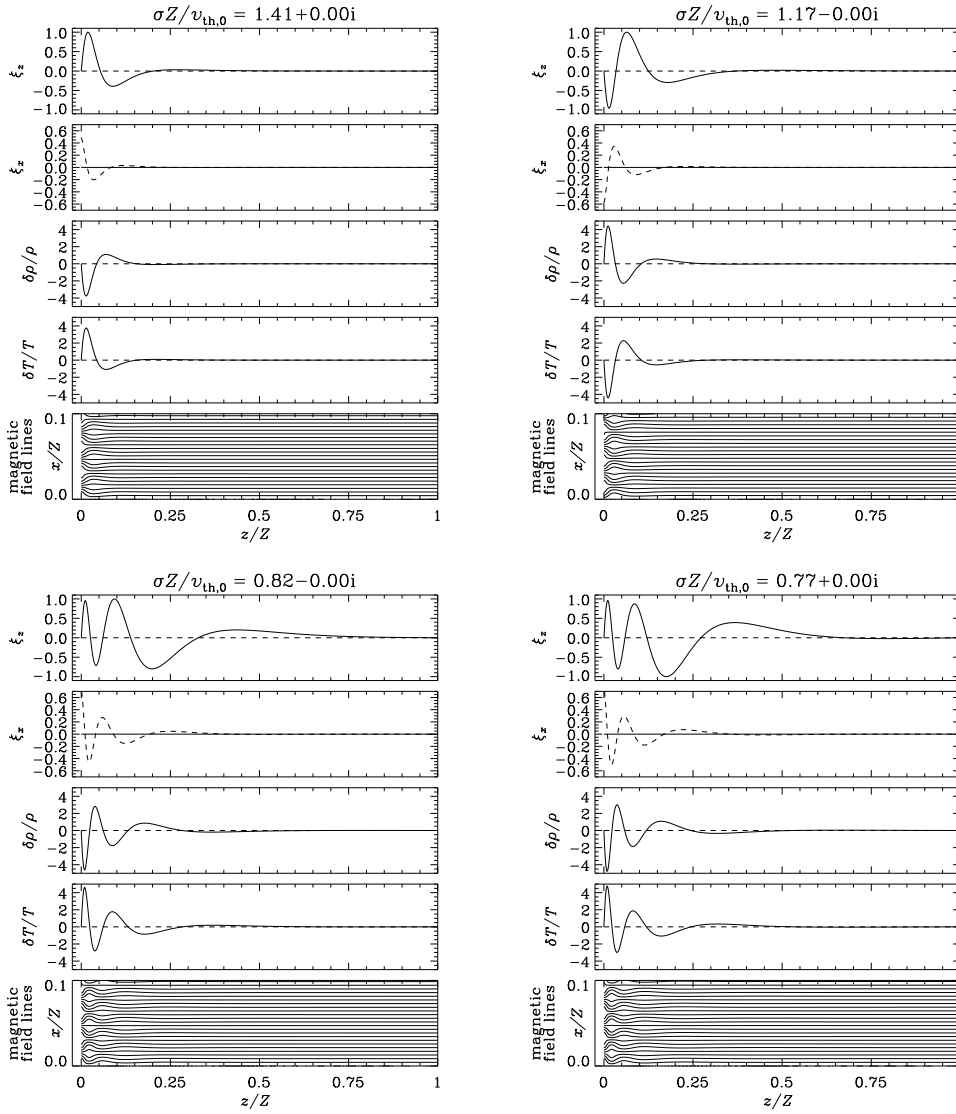


Figure 3. Eigenvectors ($\xi_x = \delta v_x/\sigma$, $\xi_z = \delta v_z/\sigma$, $\delta\rho/\rho$, $\delta T/T$) and magnetic field lines of the four fastest-growing modes for $\mathcal{S} = 0$, $\text{Kn}_0^{-1} = 1500$, $\beta_0 = 10^5$, and the horizontal wavenumber $kZ = 250$. The real (imaginary) part of each eigenvector is denoted by the solid (dashed) line. The growth rates are given at the top of each plot; for reference, $Z/v_{\text{th},0} \approx 400$ Myr for $Z = 250$ kpc and $k_{\text{B}}T_0 = 2$ keV.

of significant magnetic structures at large z is relatively slow, with e-folding times of at least 5 Gyr.

4.4 Comparison with simulations

Other than elucidating the nature of the HBI under global cluster conditions, the above analysis also serves as a useful testbed for numerical codes that include anisotropic conduction and viscosity. In this subsection we offer a comparison of non-radiative HBI growth rates computed from the linear theory (Section 4.3.1) and from simulations using the Godonov code Athena (Stone et al. 2008) equipped with a Braginskii stress and anisotropic heat conduction. Specifically, we use the simulation run ‘H2dBrag’ presented in § 4.3 of Kunz et al. (2012).

The simulation was initialized with an atmosphere identical to that denoted by the red lines in Fig. 1 with parameters the same as in Fig. 3, i.e. $\beta_0 = 10^5$ and $\text{Kn}_0^{-1} = 1500$. Likewise, the bound-

ary conditions on the top and bottom of the computational domain, which employed 512×1024 zones to span $H_0 \times 2H_0$, were the same as those described in Section 4.1.1. The equilibrium state was broken by seeding the velocity with small-amplitude white noise. Further details regarding this simulation may be found in §§ 3–4 of Kunz et al. (2012).

In Fig. 5, we superimpose the numerical dispersion relation (asterisks) on the analytical dispersion relation for the two fastest-growing modes. The numerical growth rates were obtained by Fourier transforming a periodic reconstruction of the simulation domain, selecting prominent and easily identifiable modes, and tracing their evolution throughout the linear phase of growth ($tv_{\text{th},0}/Z \approx 2\text{--}5$). The agreement between the code results and the analytical prediction is extremely good, up to wavenumbers approaching those associated with the grid spacing ($k_{\text{max}} = 1024\pi$). The corresponding real-space profiles of the temperature and density fluctuations (not shown here) are also in remarkable agreement

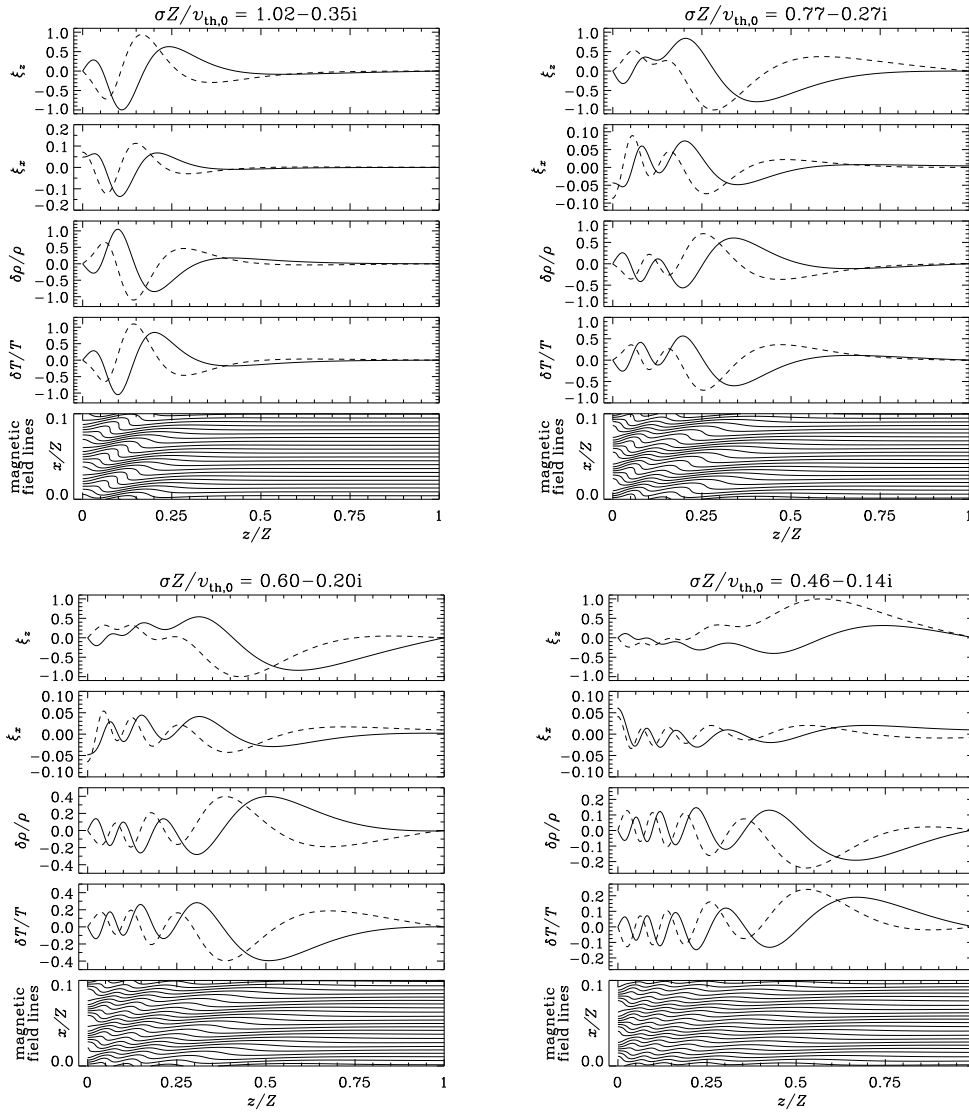


Figure 4. Eigenvectors ($\xi_x = \delta v_x/\sigma$, $\xi_z = \delta v_z/\sigma$, $\delta\rho/\rho$, $\delta T/T$) and magnetic field lines of the four fastest-growing modes for a cooling atmosphere. Parameters are the same as in Fig. 3 except that $S = 45$. These modes occur in complex conjugate pairs, but we plot only one member of each pair.

with those predicted in Fig. 3. This is a valuable check and cross-validates both the linear theory and the numerical code.

Because of numerical dissipation on the grid, at $k \gtrsim k_{\text{max}}/2$ the numerical growth rates abruptly depart from the theoretical prediction and drop precipitously. At which k this ‘unphysical’ regularisation occurs depends entirely on the resolution adopted, and formally such simulations can never be resolved. In practice, however, it is unclear how many of these small-scale HBI modes are actually required to adequately describe the nonlinear dynamics of the system. Also unclear is whether the grid regularisation realistically approximates regularisation by FLR effects, and if this matters in the saturated state. Some of these issues are addressed in Kunz et al. (2012).

5 DISCUSSION

In this paper we have examined the linear stability of weakly collisional, thermally stratified atmospheres in which the conduction of

heat and the viscous dissipation of motions are anisotropic with respect to the magnetic field. Such atmospheres are representative of those found in the cooling cores of non-isothermal galaxy clusters, which are subject to a heat-flux buoyancy-driven instability (HBI).

Numerical simulations of the HBI have established that the instability acts in such a way as to disrupt the conductive flow of heat, ultimately insulating the core from the hot thermal bath at large radii. In the presence of appreciable radiative losses, a cooling flow inevitably develops unless turbulent stirring by other means can reopen the field lines and reinstate the conductive flux.

The pressure anisotropies generated by the HBI play an important role in suppressing the instability by reducing growth rates and by shifting the fastest-growing modes to relatively long wavelengths. In the bulk of cool-core clusters, the collisionality is sufficiently low that these wavelengths become comparable to the thermal-pressure scale height of the gas. The HBI then operates on a global scale, and the analysis we have performed here marks one contribution towards understanding how the HBI changes in a global setting.

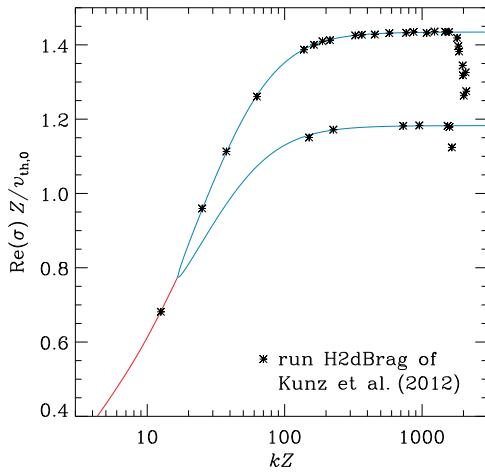


Figure 5. Comparison between the analytical dispersion relation (red and blue lines; as in Fig. 3) and the numerical dispersion relation (asterisks; obtained from run H2dBrag of (Kunz et al. 2012) for the two fastest-growing modes. The parameters of the system are: $T_Z/T_0 = 2.5$, $\mathcal{G} = 2$, $\beta_0 = 10^5$, and $\text{Kn}_0^{-1} = 1500$.

Our main result is that the low collisionality beyond ~ 50 kpc in typical cool-core clusters significantly impedes the otherwise disordered motions driven by the HBI. As a result, the magnetic-field lines can remain relatively straight over a significant fraction of the Hubble time and the conductive flow of heat may proceed at an appreciable fraction of the Spitzer value. Near-complete field-line insulation due to the HBI could very well occur, but our analysis suggests that it is well-localised to the innermost regions of the cool core. This highlights the need for radio-mode feedback at these scales from a powerful central dominant galaxy.

This conjecture is supported by recent numerical simulations of the HBI presented in Kunz et al. (2012), which self-consistently take into account the pressure anisotropy driven by the HBI and its adverse consequences for the instability's development. In contrast, Parrish et al. (2012, hereafter P12) perform analogous simulations of the HBI but these show that pressure anisotropy has little effect on the nonlinear saturation of the instability; the HBI operates throughout the bulk of the cluster core unhampered and imposes significant field-line insulation throughout. These very different conclusions possibly arise from dissimilar parameters and models. In particular, the P12 simulations that employ a plane-parallel atmosphere are of very small vertical extent, typically $Z = 0.2H_0$. As a consequence, there is insufficient room for global effects to come into play. These simulations cannot exhibit the mode localisation that we emphasise. However, P12 also perform two spherical global simulations of the HBI in model cool-core clusters, and these support the results of their plane-parallel simulations. Here the contradiction with our work is more puzzling, but probably arises from different parameters. For instance, P12's ICM model is far more collisional and less magnetised than ours, with $\beta \sim 10^7$. The effective absence of magnetic tension in these simulations may be important as magnetic tension suppresses those shorter-scale (local) HBI modes that function throughout the core. Alternatively, the discrepancy may be due to P12's different initial magnetic-field geometry (tangled on scales 30–50 kpc) or due to a basic dissimilarity between the spherical and plane-parallel geometries. But the apparent disagreement is a spur for future work: further three-dimensional simulations of cool-core clusters under representative conditions are needed.

ACKNOWLEDGMENTS

The authors would like to thank the reviewer, Steve Balbus, for an insightful review that helped clarify a number of issues in the manuscript. HNL acknowledges funding from STFC through grant ST/G002584/1. MWK was supported by STFC grant ST/F002505/2 during the early phases of this work and is currently supported by NASA through Einstein Postdoctoral Fellowship Award Number PF1-120084 issued by the Chandra X-ray Observatory Center, which is operated by the Smithsonian Astrophysical Observatory for and on behalf of NASA under contract NAS8-03060. This work was supported in part by the Leverhulme Trust Network for Magnetised Plasma Turbulence. The authors thank Alex Schekochihin for many beneficial conversations and for reading through an earlier draft of the manuscript.

REFERENCES

- Balbus S. A., 2000, *ApJ*, 534, 420
- Balbus S. A., 2001, *ApJ*, 562, 909
- Balbus S. A., Reynolds C. S., 2008, *ApJ*, 681, L65
- Bogdanović T., Reynolds C. S., Balbus S. A., Parrish I. J., 2009, *ApJ*, 704, 211
- Boyd J. P., 2000, *Chebyshev and Fourier Spectral Methods* (2nd ed.), Dover Publications, New York.
- Braginskii S. I., 1965, *Rev. Plasma Phys.*, 1, 205
- Brandenburg A., Jennings R. L., Nordlund A., Rieutord M., Stein R. F., Tuominen I., 1996, *JFM*, 306, 325
- Carilli C. L., Taylor G. B., 2002, *ARA&A*, 40, 319
- Catto P. J., Simakov A. N., 2004, *Phys. Plasmas*, 11, 90
- Cavagnolo K. W., Donahue M., Voit G. M., Sun M., 2009, *ApJS*, 182, 12
- Chew C. F., Goldberger M. L., Low F. E., 1956, *Proc. R. Soc. London A*, 236, 112
- Golub G. H., van Loan C. F., 1996. *Matrix Computations*, John Hopkins Uni. Press, Baltimore USA
- Hurlburt N. E., Proctor M. R. E., Weiss N. O., Brownjohn D. P., 1989, *JFM*, 207, 587
- Kunz M. W., 2011, *MNRAS*, 417, 602
- Kunz M. W., Bogdanović T., Reynolds C. S., Stone J. M., 2012, *ApJ*, in press
- Lamb H., 1997, *Hydrodynamics*, Cambridge Uni. Press, Cambridge UK
- McCourt M., Parrish I. J., Sharma P., Quataert E., 2011, *MNRAS*, 413, 1295
- Parrish I. J., McCourt M., Quataert E., Sharma P., 2012, 422, 704
- Parrish I. J., Quataert E., 2008, *ApJ*, 677, L9
- Parrish I. J., Quataert E., Sharma P., 2009, *ApJ*, 703, 96
- Parrish I. J., Quataert E., Sharma P., 2010, *ApJ*, 712, L194
- Peterson J. R., Fabian A. C., 2006, *Phys. Rep.*, 427, 1
- Proctor M. E. P., Weiss N. O., 1982, *RPPH*, 45, 1317
- Quataert E., 2008, *ApJ*, 673, 758
- Ruszkowski M., Oh S. P., 2010, *ApJ*, 713, 1332
- Rybicki G. B., Lightman A. P. 1979, *Radiative Processes in Astrophysics*. Wiley, New York
- Schekochihin A. A., Cowley S. C., Kulsrud R. M., Hammett G. W., Sharma P., 2005, *ApJ*, 629, 139
- Schekochihin A. A., Cowley S. C., Rincon F., Rosin M. S., 2010, *MNRAS*, 405, 291
- Spitzer L. Jr., 1962, *Physics of Fully Ionized Gases*. Wiley Interscience, New York, NY

Stone J. M., Gardiner T. A., Teuben P., Hawley J. F., Simon J. B.,
2008, *ApJS*, 178, 137